Table of contents:

S1 Monte Carlo radiative transfer model

The Monte Carlo method solves the radiative transfer equation (RTE) by simulating large ensembles of photon events represented by random samples from probability density functions (Ertürk and Howell, 2017). In this study and others, the Monte Carlo method is used to quantify relative uncertainties in imperfect optical measurements that are intractable with analytical or numerical solutions to the RTE (Gordon, 1985). We developed a Monte Carlo radiative transfer model to estimate the effect of detector interference on our irradiance measurements. The model closely follows methods developed to simulate light propagation in biological tissue, ocean waters, and sea ice (Leathers et al., 2004; Light et al., 2003; Wang et al., 1995). A general description of the model and particular modifications for this investigation are described below.

S1.1 Probability functions for optical properties

The fundamental ingredients of this and other Monte Carlo radiative transfer models are the inherent optical properties k, ω, and g (see Sect. 2.3 of the main), the geometric boundary conditions, and the probabilistic rules that govern the system. The cumulative probability of occurrence for an event x, with probability density function $\mathrm{p(x)}$, is:

$$\mathrm{P(x)} = \int_{-\infty}^{\mathrm{x}} \mathrm{p(x)dx}, \quad 0 \leq \mathrm{P(x)} \leq 1. \tag{1}$$

To solve for x, the left-hand-side (LHS) of (1) is replaced with a random number:

$$\mathrm{P(x)} = q \tag{2}$$

where q is from the uniform distribution over [0,1]. The right-hand-side (RHS) lower limit of integration $-\infty$ is replaced with an appropriate limit (e.g., 0) and analytic or empirical expressions for $\mathrm{p(x)}$ are specified.

In this study, x represents optical path length, scattering direction, and photon survival probability. Closed-form expressions for each of these terms are given in the following sections.

S1.1.1 Optical path length

The probability density function for the optical path length l [$\mathrm{m^{-1}}$] is given by the e-folding length:

$$\mathrm{p}(l) = \mathrm{e}^{-l}, \qquad l \geq 0 \tag{3}$$

with the cumulative distribution function:

$$\mathrm{P}(l) = \int_0^l \mathrm{e}^{-l'}\mathrm{d}l' = 1 - \mathrm{e}^{-l}. \tag{4}$$

From Eq. (2), $q = 1 - \mathrm{e}^{-l}$ and therefore:

$$l = -\ln q\,, \qquad 0 \leq 1. \tag{5}$$

In this study, q is generated with the MATLAB function `rand`.

The photon transport length [m] is the optical path length scaled by the extinction coefficient:

$$s = l/\sigma_e \tag{6}$$

where:

$$\sigma_e = \sigma_s + \sigma_a \tag{7}$$

is the single-scattering extinction coefficient, σ_s [m^{-1}] is the scattering coefficient, and σ_a [m^{-1}] is the absorption coefficient.

S1.1.2 Scattering phase function

The probability density function for a scattering phase function with azimuthal symmetry is:

$$p(\theta_s) = 2\pi\tilde{\beta}(\theta_s)\sin\theta \tag{8}$$

where $\tilde{\beta}(\theta_s)$ is the probability that a photon will scatter at polar angle θ_s. We specify $\tilde{\beta}(\theta_s)$ with the Henyey-Greenstein scattering phase function, which is appropriate for strongly forward scattering by ice grains and air bubbles (Light et al., 2003):

$$\tilde{\beta}(g, \theta_s) = \frac{1}{4\pi}\frac{1-g^2}{(1+g^2-2g\cos\theta_s)^{\frac{3}{2}}}, \qquad -1 < g < 1. \tag{9}$$

where $g = 0$ reduces Eq. 9 to isotropic scattering and $g \to 1$ is strongly forward scattering. In this study, $g = 0.86$, as given by Mullen & Warren (1988) from Mie theory calculations for scattering by air bubbles in ice.

From Eq. (1):

$$P(\theta_s) = -\frac{1-g^2}{2}\int_0^{\theta_s}\frac{\sin\theta_s'}{(1+g^2-2g\cos\theta_s')^{\frac{3}{2}}}d\theta_s' = q \tag{10}$$

which evaluates to:

$$q = \frac{1-g^2}{2g}\left[\frac{1}{1-g} - \frac{1}{\sqrt{1+g^2-2g\cos\theta_s}}\right] \tag{11}$$

yielding the scattering angle:

$$\cos\theta_s = \frac{1}{2g}\left[1+g^2-\left(\frac{1-g^2}{1-g+2gq}\right)^2\right], \qquad g \neq 0;\ 0 \le \theta_s \le \pi/2. \tag{12}$$

The probability density function for scattering azimuth angle ϕ_s in a spherical coordinate system with azimuthal symmetry is $1/2\pi$. From Eq. (1):

$$P(\phi_s) = \frac{\phi_s}{2\pi}, \qquad 0 \le \phi_s \le 2\pi \tag{13}$$

and from Eq. (2):

$$\phi_s = 2\pi q. \tag{14}$$

S1.1.3 Photon termination

Monte Carlo simulations are computationally expensive. To improve computational performance, photons are treated as packets of photons with initial weight $w = 1$. At each interaction, photons are scattered and absorbed according to their respective statistical probabilities, parameterized by σ_s and σ_a. Accordingly, at each interaction the weight is updated as:

$$w = (1 - \overline{\omega}) \cdot w \tag{15}$$

where:

$$\overline{\omega} = \sigma_\mathrm{s}/\sigma_e \tag{16}$$

is the single-scattering albedo [-]. Each $1 - \overline{\omega}$ reduction in photon packet weight is proportional to the probability of an individual photon absorption event. After many interactions, if w drops below a very small value it contributes very little to the solution. The so-called "Russian roulette" technique is used to improve computational performance, where photon packet weights below a specified threshold $w < w_\mathrm{min}$ are increased in proportion to a survival probability function and are re-released into the medium, or otherwise terminated:

$$w = \begin{cases} \mathrm{m} \cdot w, & q \leq 1/\mathrm{m} \\ 0, & q > 1/\mathrm{m} \end{cases} \tag{17}$$

where $1/\mathrm{m}$ is the probability of photon survival and q is a random number as previously defined. This technique conserves energy and is unbiased (Wang et al., 1995). In this study, $w_\mathrm{min} = 10^{-5}$ and $\mathrm{m} = 10$.

At each interaction, the absorbed fraction $\overline{\omega} \cdot w$ is scored into an absorption array in a cylindrical coordinate system that is used to compute observable quantities of absorption and photon fluence. If a photon packet exits the medium, it is scored into a transmittance or reflectance array in an azimuthally independent spherical coordinate system that is used to compute observable quantities of irradiance, radiant intensity, and power. These scoring systems follow the definitions in Wang et al. (1995) Eq. 4.1–4.32.

The preceding sections describe the fundamental processes of photon transport, scattering direction, and survival probability. Similar probability density functions that describe the detector rod interference are described next.

S1.2 Monte Carlo experiment

The detector rod interference is estimated with a "backward" Monte Carlo (BMC) simulation, which simulates photon trajectories starting from the detector backward to the target (Leathers et al., 2004; Light et al., 2003). Here, the target is the ice surface. The simulation domain is a 3-dimensional ice slab with one boundary, the ice surface, and otherwise infinite horizontal and vertical extent. A cylinder with dimensions identical to the detector rod is placed at positions identical to the measurement depths reported in this paper, and photon packets are released from the irradiance sensor ("remote cosine receptor") located on the detector rod (Fig. S1).

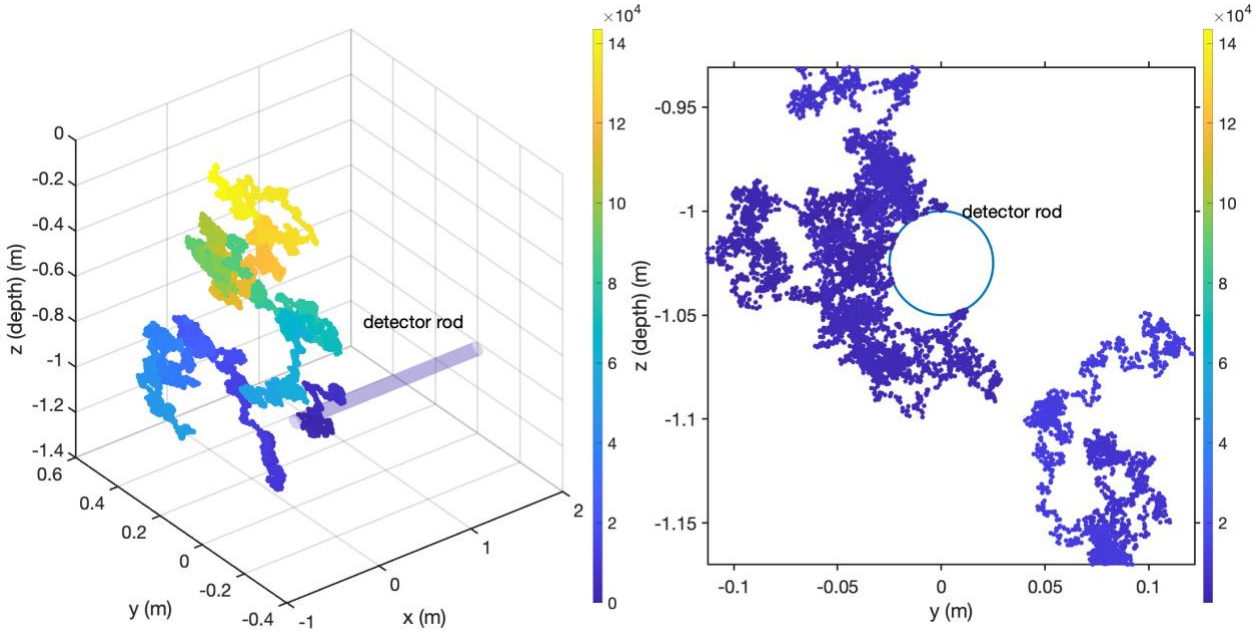

Fig. S1: Example Monte Carlo photon tracking simulation from model output used in this study, with interference by cylindrical detector rod. (a) ~14,000 random photon interactions are traced within a 3-dimensional ice volume. The cylindrical object represents the detector rod, here inserted at 1 m below the ice surface. The photon packet is released from the position of the irradiance sensor ("remote cosine receptor") located on the rod and traced backward to the ice surface ("backward Monte Carlo"). (b) Magnified view of the detector rod in the y-z plane shows photon packets scattering off of the rod. The color-bar represents the number of cumulative interactions experienced by this photon packet.

As described above, each interaction within the ice volume is defined by absorption and scattering of the photon by ice. Absorption reduces the photon energy density by an amount $1 - \overline{\omega}_{\mathrm{ice}}$. Scattering redirects the photon trajectory according to the Henyey-Greenstein scattering phase function with asymmetry parameter g and transport distance l. Photon interactions with the detector rod require additional specifications that are described next.

S1.2.1 Source function for cosine detector

The scattering phase function for an irradiance sensor with a cosine response is:

$$\tilde{\beta}(\theta) = \frac{\cos\theta}{\pi}, \qquad 0 \le \theta \le \frac{\pi}{2} \tag{18}$$

with probability density function:

$$p(\theta) = 2\pi\tilde{\beta}(\theta)\sin\theta \tag{19}$$

and cumulative distribution function:

$$P(\theta) = 2\int_0^{\theta} \cos\theta' \sin\theta' \, d\theta' = q\,. \tag{20}$$

Substituting $\mu = \cos(\theta)$ the scattering angle is:

$$\cos\theta = \sqrt{1-q}. \tag{21}$$

For a forward Monte Carlo simulation, Eq. 21 gives the probability of photon receipt by an irradiance sensor with an ideal cosine response. For a BMC simulation, the form of Equation 21 that gives the initial launch trajectory of photons from the irradiance sensor surface is:

$$\cos\theta = -\sqrt{q}. \tag{22}$$

In reality, irradiance sensors do not have an ideal cosine response to radiance. In this experiment, the non-ideal cosine response of the irradiance sensor is estimated by replacing Eq. 22 with uniform sampling from an empirical probability density function derived from laboratory measurements of the cosine receptor angular response function provided by Ocean Optics (Fig. S2). The source azimuth angle ϕ is determined with Eq. (14).

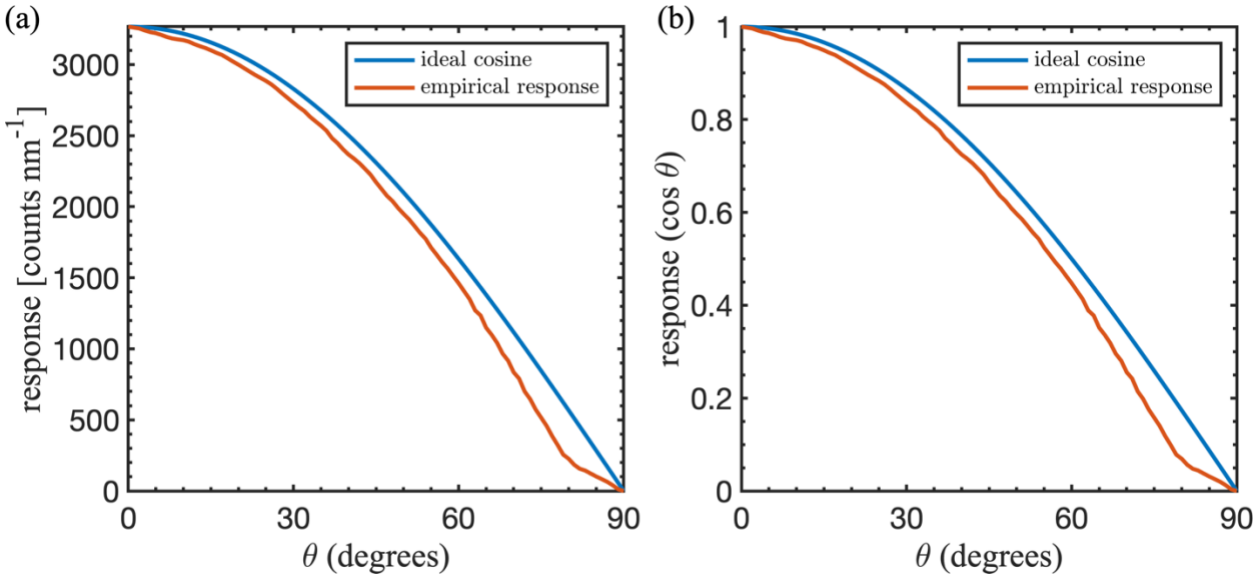

Fig. S2: (a) Comparison of ideal angular response function (ideal cosine) with the empirical angular response function used to estimate the non-ideal response of the irradiance sensor used in this study. The empirical angular response function was developed by Ocean Optics from laboratory measurements on the same irradiance sensor type used in this study. (b) Same as (a) but normalized. The red line in (b) is the empirical probability density function used as the irradiance source function for our backward-Monte Carlo simulations (see Eq. 21–22).

S1.2.2 Scattering and absorption by detector rod

If a photon trajectory crosses the 3-dimensional position of the detector rod, the photon energy density is reduced by an amount $1 - \omega_{\text{rod}}$ and the photon is scattered away from the rod (Fig. S1) with an isotropic scattering phase function:

$$\theta_s = 1 - 2q, \tag{23}$$

$$\phi_s = 2\pi q. \tag{24}$$

The collision point is determined with ray tracing formulas that equate the vector equation of the photon trajectory with the parametric equation for the cylindrical detector rod surface following Ertürk and Howell (2017) Sect. 7.1 Eq. 59–66.

The polyvinyl chloride (PVC) detector rod albedo ω_{rod} is estimated from values for the complex refractive index of PVC (Zhang et al., 2020). Let $\mu = \cos\theta$ be the cosine zenith angle of incident radiation with $\mu = +1$ vertically

downward. Following Modest (2013) Section 2.5 Eq. 2.89–2.98, the Fresnel reflectivity and transmissivity to incident (downward) radiation are:

$$R_{\mathrm{F}}(\mu) = \frac{1}{2}\left[\left(\frac{\mu - \mathrm{n}\mu_{\mathrm{n}}}{\mu + \mathrm{n}\mu_{\mathrm{n}}}\right)^2 + \left(\frac{\mathrm{n}\mu - \mu_{\mathrm{n}}}{\mathrm{n}\mu + \mu_{\mathrm{n}}}\right)^2\right] \tag{25}$$

$$T_{\mathrm{F}}(\mu) = 1 - R_{\mathrm{F}}(\mu) \tag{26}$$

where $\mathrm{n} + \mathrm{ik}$ and $\mathrm{n}_0 + \mathrm{ik}_0$ are the complex refractive indices of PVC and air, respectively, and:

$$\mu_{\mathrm{n}} = \sqrt{1 - (1 - \mu^2)/\mathrm{n}^2} \tag{27}$$

is the refracted cosine zenith angle in the PVC pipe. Radiation transmitted into the PVC is attenuated exponentially:

$$\mathrm{a}(\mu_{\mathrm{n}}) = \mathrm{e}^{-\tau/\mu_{\mathrm{n}}} \tag{28}$$

where:

$$\tau = 4\pi kL/\lambda \tag{29}$$

is the optical thickness of the PVC pipe with wall thickness $L = 0.004$ m. Radiation that transmits through L is internally reflected upward from the inner wall in the direction μ_{n} and attenuated exponentially along path length τ. Radiation that reaches the outer wall at $\mu_{\mathrm{n}} < \mu_{\mathrm{c}}$ is transmitted across the outer wall according to $T_{\mathrm{F}}(\mu_{\mathrm{n}})$ and reflected back into the PVC according to $R_{\mathrm{F}}(\mu_{\mathrm{n}})$, where μ_{c} is the critical angle given by Snell's law:

$$\mu_{\mathrm{c}} = \sqrt{1 - 1/\mathrm{n}^2}. \tag{30}$$

Formulas for $T_{\mathrm{F}}(\mu_{\mathrm{n}})$ and $R_{\mathrm{F}}(\mu_{\mathrm{n}})$ are similar to Eq. 25 and Eq. 26 with modifications for total internal reflection about μ_{c} and are given elsewhere (Briegleb and Light, 2007; Liou, 2002).

The total reflectivity is estimated with the successive-order-of-scattering method (van de Hulst, 1980), which accounts for the multiple internal reflections and absorption within the PVC described by Eq. 25–30. We model the PVC pipe as a plane, which is justified because the radius of curvature is much larger than all wavelengths of light considered here. For the geometry and optical properties of the detector rod, the total reflectivity has the closed-form solution:

$$R_{\mathrm{d}} = R_{F,\mu} + \frac{T_{F,\mu} R_{F,\mu_{\mathrm{n}}} T_{F,\mu_{\mathrm{n}}} \mathrm{a}_{\mu_{\mathrm{n}}}^2}{1 - R_{F,\mu_{\mathrm{n}}} a_{\mu_{\mathrm{n}}}^2} \tag{31}$$

where the subscripts μ and μ_{n} on R, T, and a indicate the direction of incident radiance.

S2 Model validation

The Monte Carlo model described above is verified by comparison with benchmark values for total diffuse reflectance R_{d} [W m^{-2}], total transmittance T_{t} [W m^{-2}], diffuse angular reflectance $R_{\mathrm{d}}(\alpha)$ [W sr^{-1}] and diffuse angular transmittance $T_{\mathrm{d}}(\alpha)$ [W sr^{-1}] tabulated by van de Hulst (1980). The angular quantities, which have units of radiant intensity, are defined with respect to the exiting angle normal to the surface α [rad]. For a plane-parallel slab with optical properties $\sigma_{\mathrm{s}} = 0.9$ m^{-1}, $\sigma_{\mathrm{a}} = 0.1$ m^{-1}, $\mathrm{g} = 0.75$, and optical thickness $\tau = 2$, the van de Hulst (1980) solutions are $R_{\mathrm{d}} = 0.09739$ and $T_{\mathrm{t}} = 0.66096$. For an ensemble of $N = 100$ simulations, the Monte Carlo model described

above gives $R_{\mathrm{d}} = 0.09740 \pm 0.00034$ and $T_{\mathrm{t}} = 0.66098 \pm 0.00049$ ($\mu \pm 1\sigma$). The model closely reproduces the benchmark solutions for $R_{\mathrm{d}}(\alpha)$ and $T_{\mathrm{d}}(\alpha)$ (Fig. S3).

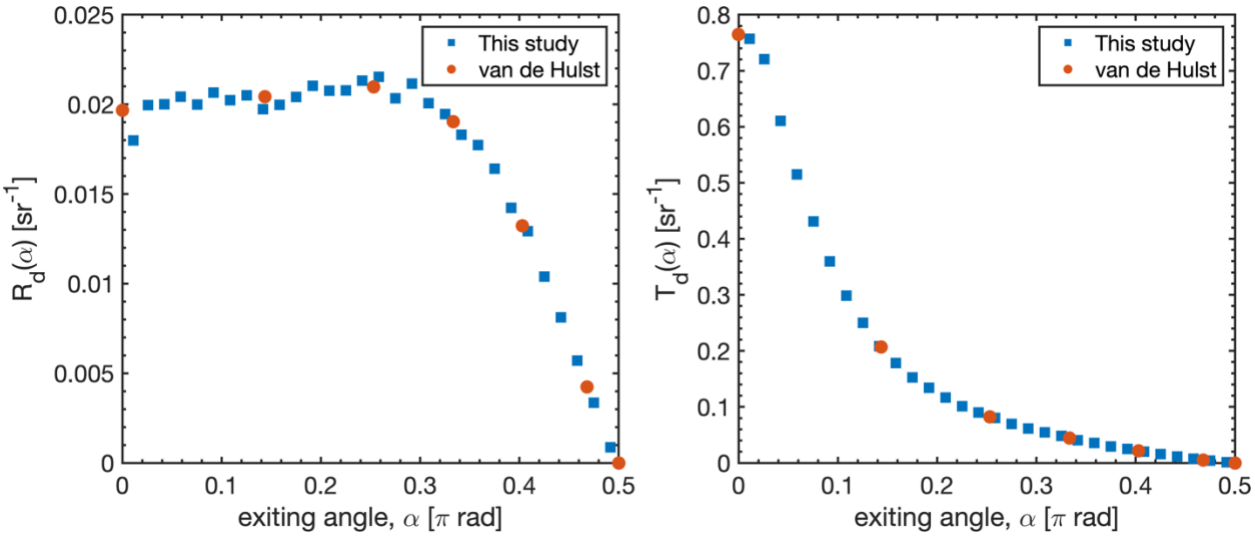

Fig. S3: Values of diffuse angular reflectance (radiant intensity), $R_d(\alpha)$ and transmittance $T_d(\alpha)$ vs. the photon exiting angle with respect to the surface normal α (after Wang et al. 1995 Fig. 3). Solid circles are benchmark solutions from Table 35 in van de Hulst (1980), obtained with the doubling method of solution to the radiative transfer equation.

S3 Monte Carlo uncertainty estimate

The Monte Carlo model is used to estimate the effect of detector interference on our irradiance measurements and, in turn, the asymptotic flux attenuation coefficients k_{att} that are estimated from them. To this end, we designed four experiments that isolate two forms of detector interference: 1) the non-ideal cosine response of the irradiance detector, and 2) absorption and scattering by the PVC detector rod. The four experiments, including a base simulation with no detector interference, are summarized in Table S1.

Table S1: Summary of four Monte Carlo experiments that simulate the effect of the detector rod interference on in-ice irradiance measurements. The baseline simulation (ideal diffusion, no rod) has no detector interference.

Experiment	Source function	Detector absorption	Detector scattering
Ideal Diffusion, No Rod	Eq. 23-24	-	-
Ideal Cosine, No Rod	Eq. 22	-	-
Ideal Cosine, With Rod	Eq. 22	ω_{rod}	Eq. 23-24
Non-ideal Cosine, With Rod	Empirical (Fig. S2)	ω_{rod}	Eq. 23-24

For each experimental setup, the Monte Carlo is integrated across 10,000 interactions at four wavelengths (400 nm, 500 nm, 600 nm, and 700 nm) with detector rod positions that are identical to the measurement depths reported in this paper (c.f. Fig. S1). For the 20 July experiment, these depths are 9.35 cm, 30.0 cm, 50.45 cm, and 68.60 cm, in units of solid-ice equivalent (i.e., physical thickness scaled by measured ice density). For the 21 July experiment, these

depths are 45.93 cm, 58.98 cm, 73.40 cm, and 114.5 cm. Monte Carlo k_{att} values are estimated for each wavelength with the same method used for the field-estimates, i.e., by least-squares linear regression:

$$-\log T(\mathrm{z},\lambda) = T_0 + k_{\mathrm{att}}(\lambda)\mathrm{z} + \varepsilon \tag{32}$$

where T is the total diffuse transmittance from Monte Carlo simulation (see Section S2), T_0 is a parameter (y-intercept) that represents $T(\mathrm{z}=0)$ and ε is an error term.

These simulations provide two measures of k_{att} uncertainty: 1) the difference between the average Monte Carlo k_{att} value μ_{MC} and the field-estimated k_{att} value at each wavelength, and 2) the spread among Monte Carlo k_{att} values at each wavelength. The spread among Monte Carlo k_{att} values is an estimate of uncertainty due to the irradiance sensor angular response function and the detector rod interference. The spectrometer dark-light sensitivity is an additional source of instrumental uncertainty that is estimated from field measurements as described in Sect. X. These instrumental uncertainties (irradiance sensor angular response, detector rod interference, and dark-light sensitivity) are compared with the statistical variations in the high-frequency irradiance measurements and with the statistical uncertainty in the k_{att} linear regression model (Eq. 32).

If we take the spread among the Monte Carlo k_{att} values as independent of the uncertainty estimates obtained from analysis of field datasets and the uncertainty in the linear regression model, a combined uncertainty is estimated as:

$$\varepsilon = \sqrt{\varepsilon_{MC}^2 + \varepsilon_D^2 + \varepsilon_{2\sigma}^2 + \varepsilon_{LM}^2} \tag{33}$$

where ε_{MC}, ε_D, $\varepsilon_{2\sigma}$, and ε_{LM} are the uncertainty from Monte Carlo, dark-current sensitivity, high-frequency statistical variability, and linear model statistical uncertainty, defined as one standard error in the k_{att} linear regression (Fig. S4).

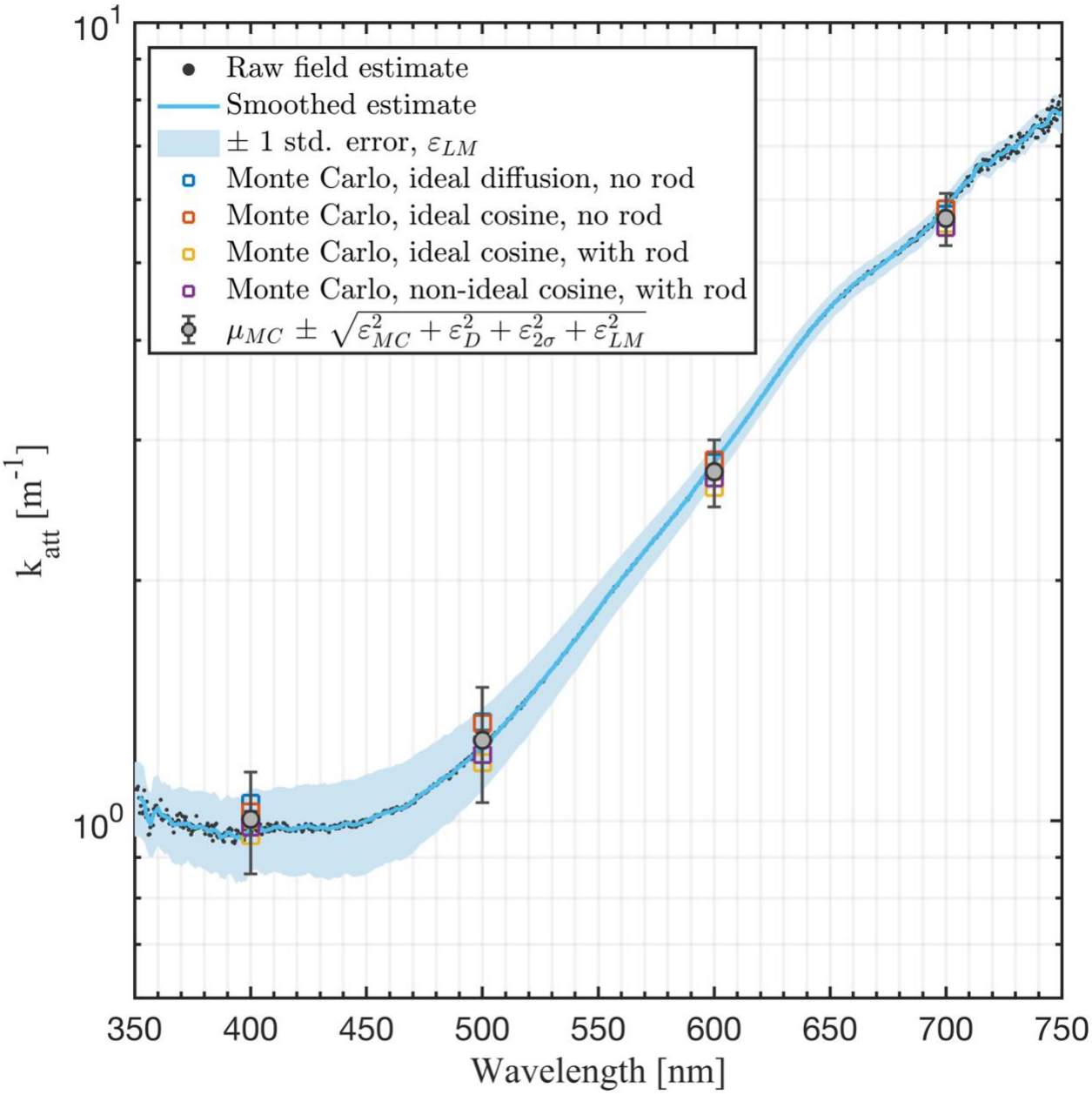

Fig S4: Attenuation coefficient k_{att} spectra from measurements of light transmission collected on 20 July, 2018, compared with average k_{att} values from four simulations with a 3-dimensional Monte Carlo radiative transfer model (μ_{MC}) and with two measures of uncertainty: 1) statistical linear model uncertainty ε_{LM} (shaded uncertainty bounds; ±1 standard error in the linear regression) and, 2) ε_{LM} combined with instrumental and measurement uncertainty (error bars; $\mu_{MC} \pm \varepsilon$). The combined estimate combines ε_{LM} with uncertainty due to spectrometer dark-light sensitivity, non-ideal cosine response of the irradiance sensor, detector rod interference, and statistical variations in the high-frequency raw data (±2 standard deviations).

References

Briegleb, B. P. and Light, B.: A Delta-Eddington Mutiple Scattering Parameterization for Solar Radiation in the Sea Ice Component of the Community Climate System Model, Technical Note, National Center for Atmospheric Research, Boulder, Colorado. [online] Available from: http://dx.doi.org/10.5065/D6B27S71 (Accessed 18 February 2019), 2007.

Ertürk, H. and Howell, J. R.: Monte Carlo Methods for Radiative Transfer, in Handbook of Thermal Science and Engineering, edited by F. A. Kulacki, pp. 1–43, Springer International Publishing, Cham., 2017.

Gordon, H. R.: Ship perturbation of irradiance measurements at sea 1: Monte Carlo simulations, Appl. Opt., 24(23), 4172, doi:10.1364/AO.24.004172, 1985.

van de Hulst, H. C.: Multiple light scattering: tables, formulas, and applications, Academic Press, New York., 1980.

Leathers, R. A., Downes, T. V., Davis, C. O. and Mobley, C. D.: Monte Carlo Radiative Transfer Simulations for Ocean Optics: A Practical Guide, Memorandum, Naval Research Laboratory, Washington, D.C. [online] Available from: https://www.oceanopticsbook.info/packages/iws_l2h/conversion/files/Leathersetal_NRL2004.pdf (Accessed 11 October 2020), 2004.

Light, B., Maykut, G. A. and Grenfell, T. C.: A two-dimensional Monte Carlo model of radiative transfer in sea ice, J. Geophys. Res. Oceans, 108(C7), 3219, doi:10.1029/2002JC001513, 2003.

Liou, K.-N.: An introduction to atmospheric radiation, 2nd ed., Academic Press, Amsterdam ; Boston., 2002.

Modest, M. F.: Radiative heat transfer, Third Edition., Academic Press, New York., 2013.

Mullen, P. C. and Warren, S. G.: Theory of the optical properties of lake ice, J. Geophys. Res. Atmospheres, 93(D7), 8403–8414, doi:10.1029/JD093iD07p08403, 1988.

Wang, L., Jacques, S. L. and Zheng, L.: MCML—Monte Carlo modeling of light transport in multi-layered tissues, Comput. Methods Programs Biomed., 47(2), 131–146, doi:10.1016/0169-2607(95)01640-F, 1995.

Zhang, X., Qiu, J., Li, X., Zhao, J. and Liu, L.: Complex refractive indices measurements of polymers in visible and near-infrared bands, Appl. Opt., 59(8), 2337, doi:10.1364/AO.383831, 2020.